Gold Nanorods Dispersed in Homopolymer Films: Optical Properties Controlled by Self-Assembly and Percolation of Nanorods

Guoqian Jiang, Michael J. A. Hore, Sangah Gam, and Russell J. Composto*

Department of Materials Science and Engineering and Laboratory for Research on the Structure of Matter, University of Pennsylvania, Philadelphia, Pennsylvania 19104-6272, United States

ABSTRACT In this paper, polymer nanocomposite films containing gold nanorods (AuNRs) and poly(2-vinyl pyridine) (P2VP) have been investigated for their structure–optical property relationship. Using transmission electron microscopy (TEM), the assembly of AuNRs (7.9 nm × 28.4 nm) grafted with a P2VP brush in P2VP films is examined as a function of the AuNR volume fraction $\varnothing_{AuNRs}$ and film thickness h. For $h \sim 40$ nm, AuNRs are confined to align parallel to the film and uniformly dispersed at low $\varnothing_{AuNRs}$. Upon increasing $\varnothing_{AuNRs}$, nanorods form discrete aggregates containing mainly side-by-side arrays due to depletion–attraction forces. For $\varnothing_{AuNRs} = 2.7\%$, AuNRs assemble into a 2D network where the discrete aggregates are connected by end-to-end linked nanorods. As $\varnothing_{AuNRs}$ further increases, the polymer-rich regions of the network fill in with nanorods and rod overlap is observed. Monte Carlo simulations capture the experimentally observed morphologies. The effect of film thickness is investigated at $\varnothing_{AuNRs} = 2.7\%$, where thicker films (40 and 70 nm) show a dense array of percolated nanorods and thinner films (20 nm) exhibit mainly isolated nanorods. Using Rutherford backscattering spectrometry (RBS), the AuNRs are observed to segregate near the substrate during spin-casting. Optically, the longitudinal surface plasmon resonance (LSPR) peaks are correlated with the local orientation of the AuNRs, where side-by-side and end-to-end alignments induce blue and red shifts, respectively. The LSPR undergoes a red shift up to 51 nm as $\varnothing_{AuNRs}$ increases from 1.6 to 2.7%. These studies indicate that the optical properties of polymer nanocomposite films containing gold nanorods can be fine-tuned by changing $\varnothing_{AuNRs}$ and h. These results are broadly applicable and provide guidelines for dispersing other functional nanoparticles, such as quantum dots and carbon nanotubes.

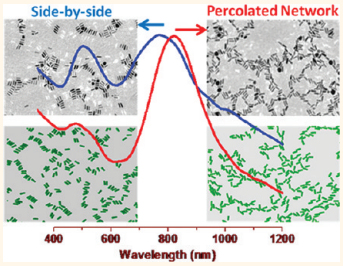

KEYWORDS: gold nanorods · poly(2-vinyl pyridine) · nanocomposite films · percolation network · transmission electron microscopy · Monte Carlo simulation · optical properties

During the past decade, polymer nanocomposites (PNCs) have attracted great interest by academic and industrial researchers. By adding a small amount of inorganic nanoparticles, such as clay, silica, metal, oxide, or carbon nanotubes,[1–6] into polymer matrices, these PNCs exhibit improved thermal, optical, electrical, magnetic, or mechanical properties. Studies of the complex physical interactions and synergy between the nanoparticles and their polymeric hosts are required if we are to understand the principles governing the improvement in the before mentioned properties. PNCs can be prepared by *in situ* synthesis of nanoparticles in polymer matrices with or without reducing agents[7–9] and *ex situ* blending of preformed nanoparticles and polymers.[10] The *ex situ* method is particularly attractive because a broad spectrum of properties can be created by exploiting many combinations of particles and polymer types.

Utilizing either attractive interactions with their host matrices or external forces, anisotropic nanorod particles have been arranged vertically or laterally onto substrates.[11–16] Thanks to their highly tunable optical properties and excellent photothermal sensitivity, gold nanorods (AuNRs) are one of the most studied anisotropic nanoparticles. Therefore, AuNRs are widely used components in medical imaging, cancer treatment, and surface-enhanced Raman scattering.[17–20] Depending on their aspect ratio, AuNRs are capable of generating surface plasmons (SPs) over a broad range covering the UV–vis–NIR region. In order to utilize their unique properties, the AuNRs must be dispersed in a host material. Polymers are extremely attractive matrices because their interface with nanoparticles can be mediated by grafting a polymer brush to the AuNRs that is similar to the matrix polymer. For example, the surface of the nanorods was grafted with a polymer brush, allowing them to be preferentially located in a lamellar domain of block copolymer films.[21–23] The energetic interactions between the nanorods with the segments in each block

* Address correspondence to composto@seas.upenn.edu.

Received for review November 22, 2011 and accepted January 27, 2012.

Published online January 27, 2012
10.1021/nn2045449

need to be precisely balanced in order to fine-tune the nanorod location, orientation, and arrangement. Moreover, the addition of nanoparticles can retard block copolymer self-assembly, leading to kinetically trapped or highly disordered structures.[24,25] By comparison, the addition of nanoparticles to homopolymers is a simple system to describe thermodynamically and dynamically if the brush is identical to the homopolymer (*i.e.*, nonattractive) or has a favorable interaction with the homopolymer.[26−28]

In addition to studies aimed at improving nanoparticle dispersion in a host, kinetically trapping the nanorods in side-by-side or network morphologies is a topic of great importance. For example, Winey *et al.*[29] has demonstrated that electrical conductivity can be remarkably enhanced when carbon nanotubes become percolated in a poly(methyl methacrylate) (PMMA) matrix. In the same system, they have also illustrated that percolation of nanotubes changes the rheological properties from liquid-like to solid-like behavior at very low nanoparticle loadings.[30] More recently, Vaia *et al.*[31] reported a highly efficient method to purify gold nanorods (*i.e.*, remove impurities) by using depletion-induced attraction forces to remove impurities from solution. Polymer-induced depletion−attraction between particles results from an attractive osmotic pressure-driven exclusion of nonabsorbing polymers located between the nanoparticles, due to a local concentration gradient.[32] In comparison with spherical nanoparticles, the critical concentration at which nanorods or nanotubes aggregate in a side-by-side manner is reduced. The aggregation behavior of nanorods is determined by many factors such as aspect ratio, size, shape, grafted brush type, and host matrix. Several theoretical studies have been conducted to illustrate the effects of nanorod or nanotube depletion−attraction on their resulting phase behavior.[33−36]

The fabrication of devices based on metal nanoparticles (nanorods) is hindered by the inherent difficulty in controlling the assembly and orientation of particles in thin films.[37] By controlling assembly of AuNRs in polymer matrices, tunable optical properties across the UV−vis−NIR region can be achieved. In this paper, we aim to understand and control the assembly of poly(2-vinyl pyridine) (P2VP) brush functionalized AuNRs in P2VP homopolymer films. By increasing $\emptyset_{AuNRs}$ at fixed film thickness (~40 nm), we observe that the dispersion of nanorods evolves from side-by-side alignment to end-to-end linking using transmission electron microscopy (TEM) and Monte Carlo simulation. A unique finding is that the discrete aggregates containing side-by-side AuNRs become connected by end-to-end linked rods to form a percolated network at $\emptyset_{AuNRs}$ = 2.7%. To the best of our knowledge, this is the first direct visualization of a gold nanorod dispersion−percolation transition in a polymer matrix. At a fixed nanorod loading, $\emptyset_{AuNRs}$ = 2.7%, distinct nanorod morphologies from well-dispersed to percolated network is observed upon increasing film thicknes. Depth profiling of the nanorods within the films obtained from Rutherford backscattering spectrometry (RBS) shows that the AuNRs segregate toward the substrate. A key finding of this study is that the optical properties of these nanocomposite films can be controlled by varying $\emptyset_{AuNRs}$. End-to-end linked nanorods lead to red shifts in the LSPR, whereas side-by-side aligned nanorods show significant blue shifts in the LSPR. By controlling nanorod assembly in a polymer matrix, new opportunities by using polymer−nanorod films as optical sensing devices are possible.

RESULTS AND DISCUSSION

Characterization of P2VP-AuNRs. The solubility of AuNRs functionalized by P2VP brushes is first tested in ethanol/H_2O, MeOH, and THF, corresponding to solvents with the highest to lowest solvent polarity index, respectively. The nanorods remain well-dispersed in all three solutions, as shown by the TEM images in Figure 1. The results qualitatively suggest that the grafting density of the P2VP brush on the AuNRs is high enough to ensure solubility in these solvents. Previous work using PEG-functionalized gold nanorods (5 kg/mol) showed that the grafting density was 0.53 chains/nm^2.[38] The grafting density for P2VP brushes (2.5 kg/mol) should be higher than this value for PEG because of its lower molecular weight. On the basis of the mass difference of gold nanorods before and after grafting with P2VP brushes, we estimate that the grafting density of the brush is ~0.86 chains/nm^2. Figure 2 shows the UV−vis spectra of the P2VP-AuNRs in MeOH, THF, and a polymer solution containing P2VP and THF. In all of the cases, the transverse SPR (TSPR) peaks are located near ~512 nm, whereas the longitudinal SPR (LSPR) peak positions are located near 800 nm. The shifts in the LSPR position are attributed to changes in the dielectric constant of the surrounding medium. For example, the LSRP peak for P2VP-AuNRs in MeOH, located near 785 nm, undergoes a red shift to 815 and 811 nm in pure THF and P2VP/THF, respectively. This nearly 30 nm red shift is likely attributed to an increase in the local refractive index of the medium. Apart from the TSPR and LSPR peaks, the broad shoulder near 550 nm is always present and is due to a low concentration (<5% by number) of larger gold nanoparticles (*i.e.*, spheres and cubes), which could not be completely removed by centrifugation.

Assembly of Nanorods in P2VP Films. *Nanorod Volume Fraction.* For nanorods grafted with a brush, their dispersion in a polymer matrix depends on several variables including the Flory−Huggins interaction parameter between matrix and brush, nanorod concentration, nanorod dimensions, and nanorod aspect

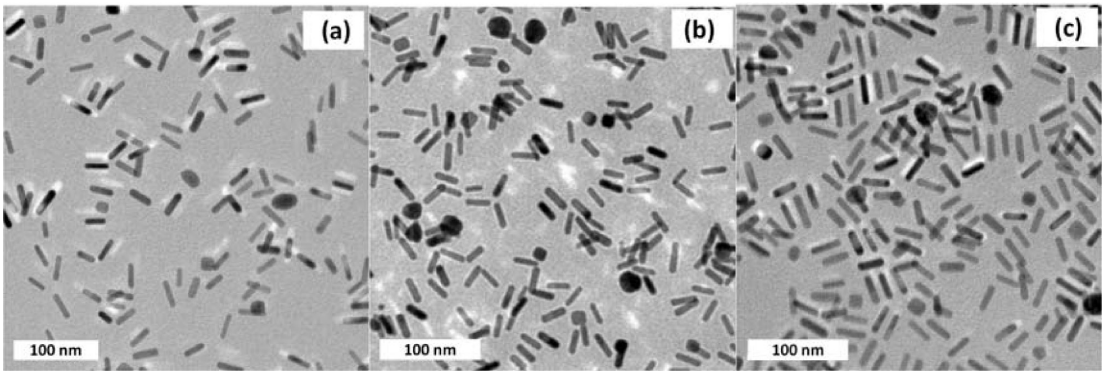

Figure 1. TEM images of as-synthesized P2VP-AuNRs deposited on a carbon-coated copper grid in (a) ethanol/H_2O; (b) methanol; and (c) THF.

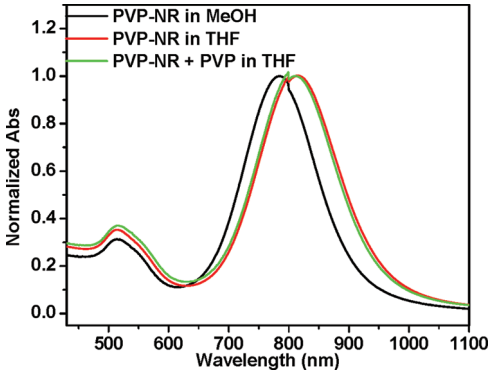

Figure 2. UV−vis spectra of P2VP-AuNRs in methanol, THF, and a polymer solution containing P2VP (5 kg/mol) and THF. The shifts of the LSPR near 800 nm are attributed to the change in the dielectric constant of the media.

ratio. Ganesan *et al.* utilized coarse-grain modeling to predict the dispersion and aggregation of nanoparticles in a polymer solution.[35,39,40] At low polymer concentrations, the pair interaction potentials between particles were found to be monotonically attractive as a function of interparticle distance. As the polymer concentration increased, the interactions deviated from monotonically attractive until a repulsive force developed at smaller interparticle distances. As the concentration increased further, a monotonically increasing repulsive interaction was observed as particles approached. These findings were in agreement with the dispersion of spherical nanoparticles[39] as well as cylindrical nanorods,[41] although the latter case was complicated by the formation of multiphases. In the present study, we aim to understand how the volume fraction of AuNRs affects the dispersion and assembly of nanoparticles in a polymer matrix.

Figure 3a−j shows TEM images for P2VP-AuNRs in P2VP films (~40 nm) at 0.4, 1.2, 1.6, 2.7, and 3.7 vol % of AuNRs ($Ø_{AuNRs}$), as well as an analysis of dispersion (right column). The film thickness is comparable to that obtained using AFM to measure the step height at a scratch (see Figure S1 in Supporting Information.) The films were obtained by spin-casting a 1.0 wt % P2VP/THF solution containing AuNRs onto silicon substrates. At $Ø_{AuNRs}$ = 0.4%, the AuNRs are well-dispersed in the matrix and appear as isolated nanorods, as shown in Figure 3a,b. When $Ø_{AuNRs}$ increases to 1.2% (Figure 3c,d), small aggregates containing side-by-side aligned nanorods appear, although a majority of the AuNRs remain isolated. Upon increasing $Ø_{AuNRs}$ to 1.6% (Figure 3e,f), the aggregates increase in size (*i.e.*, contain more AuNRs) with the nanorods retaining their side-by-side orientation; correspondingly, fewer isolated AuNRs are observed. Upon increasing $Ø_{AuNRs}$ to 2.7% (Figure 3g,h), a percolated structure is observed whereby the discrete aggregates form a network that is predominantly connected by the end-to-end linked AuNRs. In this case, the AuNRs within the aggregates appear more disordered than those at 1.6%. Although the assembly of the AuNRs evolves as $Ø_{AuNRs}$ increases up to 2.7%, the AuNRs do not cross over each other and form a monolayer. However, at $Ø_{AuNRs}$ = 3.7%, the percolated network is difficult to discern as shown in Figure 3i,j because the nanorods begin to overlap as highlighted by the circles in Figure 3j. Analysis of the TEM images at each concentration shows that the size and aspect ratio of the AuNRs are identical to those of the as-prepared nanorods shown in Figure 1. This consistency strongly suggests that the nanorods are confined by the thin film to orient parallel to the substrate, in accordance with previous studies of AuNR orientation in spun-cast PMMA-AuNRs and PS-AuNRs nanocomposite films.[26,42]

The percentage of isolated nanorods, pairs of nanorods, *etc.* are determined from analysis of TEM images using criteria based on the AuNRs' spacing and orientation. To determine the separation between AuNRs, the P2VP brush thickness, d, is estimated from the radius of gyration, R_g, using the degree of polymerization, N, and the statistical segment size, a. Assuming that a for P2VP is similar to that of polystyrene, 6.7 Å,[43] and N is 24 (M_n = 2.5K g/mol), d is determined to be ~1.3 nm if one assumes a Gaussian coil, $a(N/6)^{1/2}$. Similarly, R_g of P2VP matrix polymer (M_n = 5000 g/mol) is ~1.9 nm. Thus, for AuNRs that are as close as 3 nm, adjacent parallel nanorods are defined as *aggregated*.

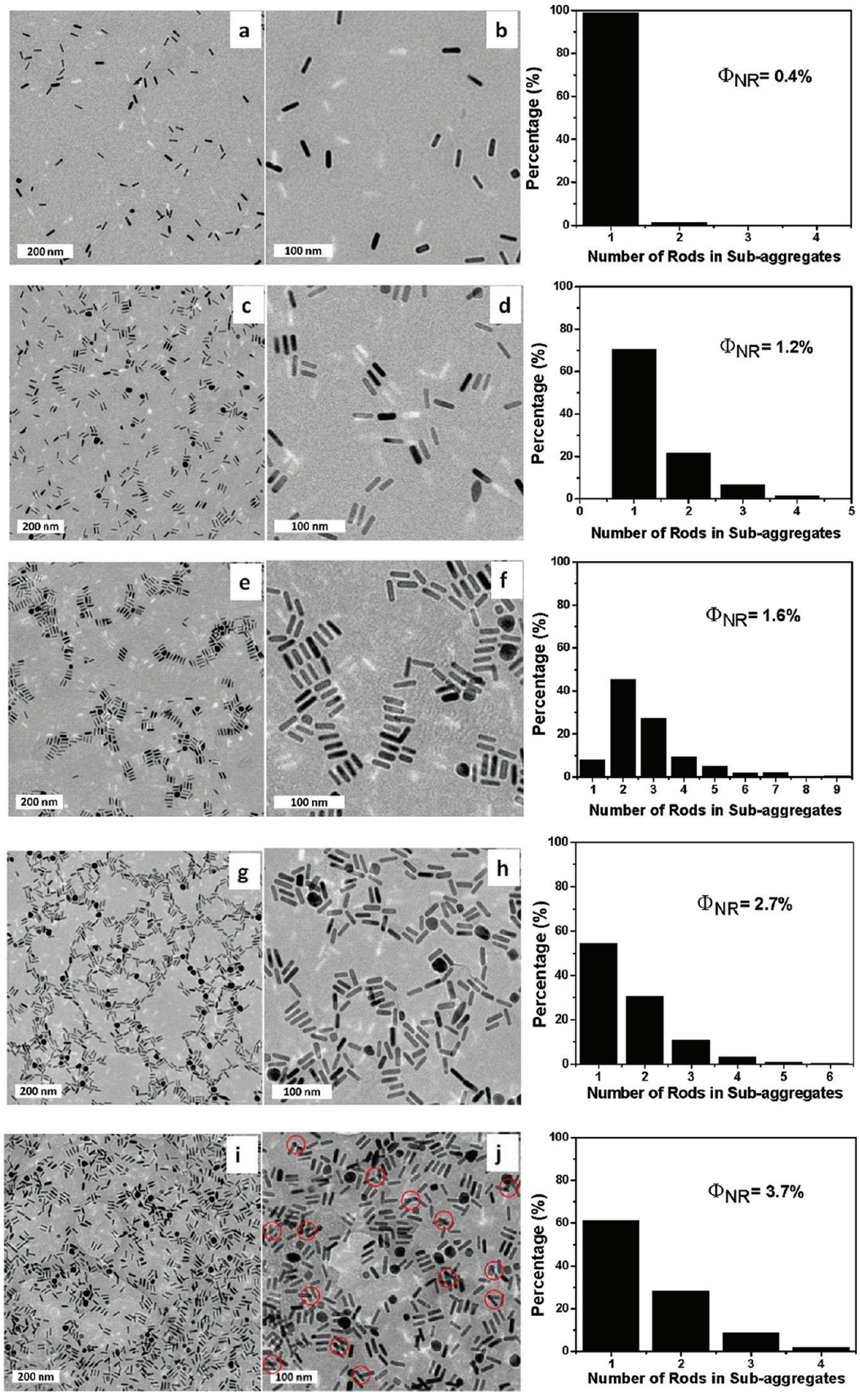

Figure 3. TEM images of films (~40 nm) spun-cast from 1.0 wt % of P2VP in solution as a function of $Ø_{AuNRs}$. $Ø_{AuNRs}$ = (a,b) 0.4%, (c,d) 1.2%, (e,f) 1.6%, (g,h) 2.7%, (i,j) 3.7%. The right column shows bar graphing giving the number of individual nanorods and nanorods in aggregates. Red circles in panel j identify overlapping nanorods. Except for $Ø_{AuNRs}$ = 0.4%, the UV−vis spectra of these films are given in Figure 7.

Furthermore, if their separation is less than 3 nm and the angle between their long axes is less than 15°, adjacent nanorods are defined as aligned in a side-by-side arrangement. Otherwise, the nanorods are considered to be *individual* particles. Thus, using this definition, we denote end-to-end aligned nanorods (*cf.*, Figure 3g,h) as two *individual* particles, even if their ends are separated by less than 3 nm. Using these criteria and assumptions, the nanorod morphology can be categorized as individual nanorods and nanorods that align in side-by-side aggregates having two, three, four, or more parallel nanorods. For each volume fraction, over 1000 AuNRs were counted to ensure statistical accuracy.

The percentages of individual and side-by-side pairs, triplets, *etc.* were determined for each $Ø_{AuNRs}$. As shown in Figure 3 (far right column), the nanorods are mainly well-dispersed and isolated at the lowest $Ø_{AuNRs}$, 0.4%, with only about 1.0% of the nanorods in side-by-side pairs. Overall, the dispersion of the AuNRs is isotropic with a low degree of orientational order. At $Ø_{AuNRs}$ = 1.2%, the percentage of individual nanorods decreases from 98.8 to 70.5%. In contrast, the percentage of the side-by-side pairs of nanorods increases from 1.2 to 21.5%. In addition, aggregates containing three and four nanorods are now observed and represent 6.5 and 1.5% of the total population, respectively. The percentage of individual nanorods decreases dramatically, from 70.5 to 8.1%, as $Ø_{AuNRs}$ increases from 1.2 to 1.6%, respectively. Correspondingly, aggregates containing two and three nanorods now account for 72.7% of the total population. Moreover, the overall aggregate size greatly increases with some aggregates containing up to nine side-by-side aligned nanorods. Aggregates containing four or more nanorods now represent 19.2% of the total at $Ø_{AuNRs}$ = 1.6%. These "aligned" aggregates (or subaggregates) tend to pack into an elongated morphology where the aggregates randomly arrange (*cf.*, Figure 3f) into larger clusters that are up to ~1 μm, as shown in Figure 3e. Whereas isotropic and nematic phases coexist at $Ø_{AuNRs}$ = 1.2%, a nematic-like phase within the aggregates is observed for $Ø_{AuNRs}$ = 1.6%.

Upon increasing $Ø_{AuNRs}$ to 2.7%, the aggregates become connected by end-to-end aligned nanorods, forming a network that spans the film. Here, the percentage of individual nanorods, including the end-to-end linked nanorods, increases to 54.5%. Correspondingly, the percentage of aggregates containing side-by-side nanorods decreases as evidenced by a noticeable decrease in the percentage of aggregates with three or more nanorods. For example, the maximum number of nanorods in a subaggregate decreases from nine to five. To the best of our knowledge, this is the first direct visualization of gold nanorod network formation in a polymer matrix. On the basis of the analysis presented in Figure 3, the critical $Ø_{AuNRs}$ for percolation is between 1.6 and 2.7%. The assembly of the AuNRs in the P2VP matrices was further examined at $Ø_{AuNRs}$ = 3.7%, above the percolation threshold. At this high volume fraction, the relative percentages of the individual and paired rods are similar to those measured at $Ø_{AuNRs}$ = 2.7%. However, the film quality was better at the lower concentration. Namely, small depressions about 10 nm deep and 100 nm wide appear throughout the films at $Ø_{AuNRs}$ = 3.7%. These depressions, which are observed in both TEM (Figure 3i,j) and AFM (Figure S2) images, may result from inhomogeneous solvent evaporation during spin-coating caused by the higher concentration of nanorods. In addition, some nanorods are observed to overlap with each other, as indicated by the circles in Figure 3j. It should be noted that the overlapping nanorods do not necessarily touch each other. Indeed, the nanorods are very likely to be placed at different heights in the films. A slight thickness increase in the nanorod-rich region may be partly responsible for the reduction in the percentage of aggregates with side-by-side nanorods. Note that for $Ø_{AuNRs} \leq$ 2.7% the nanorods are spatially distributed across nearly the same plane (*i.e.*, pseudo-2D), independent of the nanorod arrangement (*e.g.*, individual, side-by-side, or end-to-end).

Using Monte Carlo simulations, Schilling *et al.*[44] recently investigated the effect of depletion forces caused by spherical nanoparticles on the percolation networks in the suspensions of anisotropic nanotubes. From this model, the percolation threshold of carbon nanotubes with an aspect ratio of 4 was about 18% by volume. Upon adding 3 vol % of spherical micelles, the percolation threshold for the nanorods decreased by ~1 vol %. The origin of this reduction was the depletion–attraction force between nanorods induced by depleting micelles from the region between nanorods. Although higher micelle concentrations were not examined, we attribute the reduction in the percolation threshold in our study to the homopolymer-induced depletion–attraction force. There are few theoretical studies of nanorods tethered with a brush mixed with a polymer solution or matrix polymer.[35] This is primarily because the thermodynamic description of the brush–nanorod and polymer matrix system requires more parameters then in the traditional hard sphere colloidal solution system, namely, molecular weight of brush and matrix polymers and the grafting density of the brush.

Film Thickness. Using the network structure observed at a thickness of 40 nm and $Ø_{AuNRs}$ = 2.7% as a starting point, thinner and thicker films were prepared at the same volume fraction of AuNRs. Figure 4 shows TEM and AFM images for film thicknesses of 70, 40, and 20 nm. For the thickest film, h = 70 nm, similar morphology is observed as in the 40 nm thick film, where 50% of the rods are located in aggregates containing a random arrangement of nanorods. Due to the

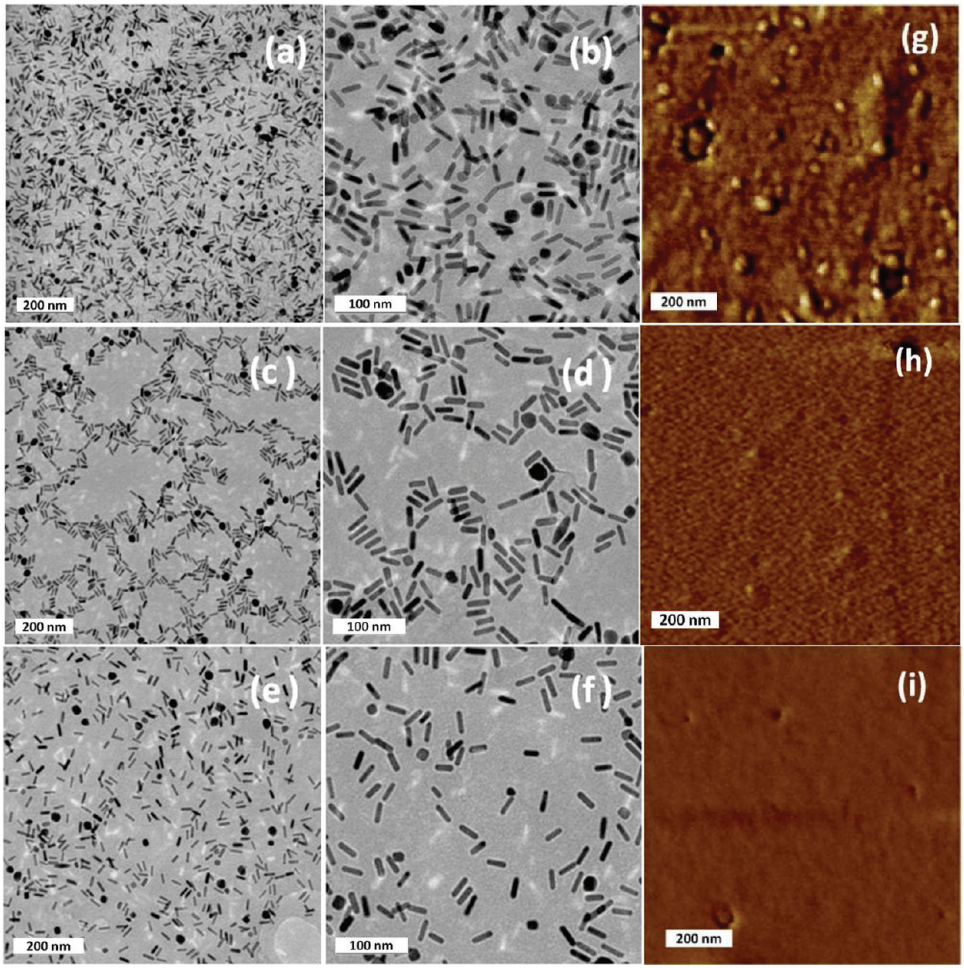

Figure 4. TEM (a–f) and AFM phase (g–i) images (0–10°) of P2VP-AuNRs in P2VP films at $Ø_{AuNRs}$ = 2.7% and film thicknesses of (a,b) 70 nm, (c,d) 40 nm, and (e,f) 20 nm. The TEM and AFM images in the left and right columns, respectively, are shown at the same magnification.

high areal density of nanorods, the structure is difficult to discern in a projected image. Analysis of the size (7.9 nm × 28.4 nm) and aspect ratio (3.6) on the nanorods in Figure 4a,b confirms that the nanorods are oriented parallel to the substrate. As previously discussed, the AuNRs form a percolated network for h = 40 nm (Figure 4c,d,h). For h = 20 nm (Figure 4e,f,i), a majority of the nanorods are isolated and dispersed, and only 16.3% of the nanorods form side-by-side pairs.

To complement the TEM studies, AFM phase images at the three film thicknesses are shown in Figure 4g–i. For the 70 nm thick film, Figure 4g shows nanorod features (~2 nm in height) protruding from the surface, suggesting that some nanorods locate near the free surface. Considering the large number of nanorods as seen from the TEM image in Figure 4a, only a very small portion of the nanorods in the film appears near the surface. For thinner films (40 and 20 nm), surface features are no longer observed, indicating that all of the nanorods are located deeper below the surface than in the thicker film. During spin-coating, solvent rapidly evaporates from the near surface, resulting in a high polymer concentration in the surface region. Consequently, nanorods segregate toward the substrate to gain entropy.[22,45] For the thinner films, the nanorods simply settle near and align with the substrate. On the other hand, the films prepared with a higher concentration of P2VP allow for a gradient in the nanorod concentration profile, and as a result, some partitioning of AuNRs near the substrate is expected.

Rutherford backscattering spectrometry (RBS) was recently used to characterize dynamics and thermodynamics in polymer films containing nanoparticles.[22,46,47] Using RBS, the depth profiles of nanorods in 200 and 100 nm thick films were measured (Figure 5). Unfortunately, films thinner than 100 nm cannot be analyzed due to the limited depth resolution. For the 100 nm film having a volume fraction $Ø_{AuNRs}$ of 3.0% (Figure 5a), the RBS profile shows a single peak located between channels 260 and 290, suggesting a "uniform" distribution of nanorods throughout the film. This result seems to contradict the previous findings that some nanorods locate near the surface of the 70 nm film containing

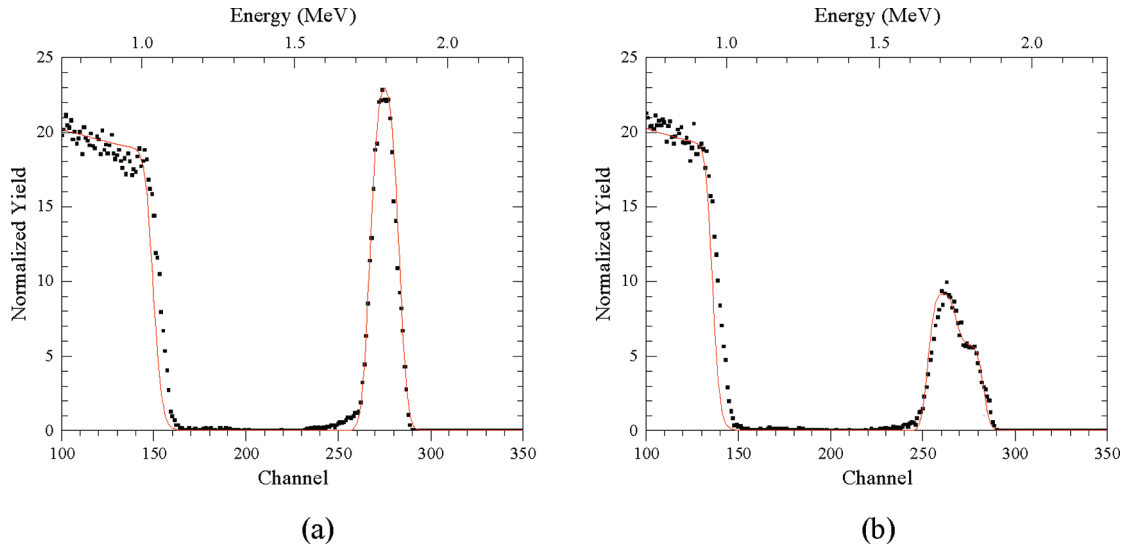

Figure 5. RBS spectra (black squares) and simulation (red lines) from P2VP-AuNRs in a P2VP film with thickness and $\emptyset_{AuNRs}$ of (a) ~100 nm and 3.0 vol %, and (b) ~200 nm and 1.0 vol %. Backscattering from Au is observed between channels 250 and 290. The yield starting at channel 150 is from the silicon substrate.

3.7 vol % of AuNRs. It might be due to the fact that RBS lacks the sensitivity to distinguish a small surface excess of AuNRs from the bulk concentration of Au.[48] The step in yield near channel 150 corresponds to backscattering from silicon atoms at the surface of the silicon substrate. For a thicker film, ~200 nm, containing 1.0% nanorods, the nanorod depth profile exhibits two distinct layers (Figure 5b). Using XRUMP[49] to analyze the spectrum, the simulation (red line) shows that the near surface region at ~100 nm is depleted of nanorods, whereas the substrate region is enriched with nanorods. Specifically, the top layer contains 0.7% of gold nanorods, whereas the bottom layer contains a higher concentration, 1.2%. The overall concentration for the entire film is ~1.0%. The higher concentration of gold nanorods near the substrate is consistent with solvent-induced segregation that occurs during spin-casting. This behavior has been previously observed in block copolymer films (~500 nm) containing nanorods.[22,45] For comparison, the XRUMP simulation for the 100 nm film shows that one layer of AuNRs at 3.0 vol % fits the experimental profile (Figure 5a, red line).

Monte Carlo Simulations. To understand the interactions that underlie the morphologies observed in Figures 3 and 4, Monte Carlo (MC) simulations were performed at three volume fractions of nanorods. The RBS spectra in Figure 5 indicate that the nanorods preferentially locate near the substrate to form a layer of nanorods of diameter $D_{rod} = 2r_{rod}$ in a film of thickness $d \sim 5(2r_{rod})$. For this reason, the effective volume fraction of AuNRs in a region of thickness $2r_{rod}$ can be approximated as

$$\emptyset^* \approx \emptyset(d/2r_{rod}) \approx 5\emptyset \quad (1)$$

This effective volume fraction is used to convert between the experimental and the equivalent MC volume fractions.

In Figure 6, the morphologies determined by MC simulations after approximately 2×10^6 MC steps (top) are compared to experimental TEM images (bottom). The MC images, from left to right, correspond to $\emptyset$ = 1.0, 15.0, and 20.0%. The TEM images, from left to right, correspond to $\emptyset$ = 0.4, 1.6, and 2.7%, or in terms of the effective volume fraction from eq 1, $\emptyset^*$ = 2.0, 8.0, and 13.5%, respectively. While a quantitative comparison between the experimental results and simulations is problematic, a qualitative comparison shows that the MC simulations are able to reproduce the structural evolution of the experimental morphologies as the AuNRs' volume fraction increases. In particular, at low volume fractions, AuNRs are mostly isolated from one another, although a small number of side-by-side aggregations are observed. As the volume fraction increases to moderate values, aggregates containing side-by-side AuNRs form and extend throughout the simulation space. Finally, at $\emptyset \geq 20\%$, a percolated-like morphology is observed, where AuNRs form both side-by-side and end-to-end arrays. The morphology ceases to evolve with further MC steps, indicating that the structure is kinetically trapped.

Optical Properties of P2VP-AuNRs/P2VP Films. One important goal of this research project is to correlate the morphology of nanorods in a polymeric film with their optical properties. As shown in Figure 7, the CTAB-modified gold nanorods in water exhibit transverse and longitudinal SPR peaks at 511 and 766 nm, respectively. The estimation of longitudinal peak position based on the discrete dipole approximation method[50] in water is given by

$$\lambda_{LSPR} = 418 + 96 \times AR \quad (2)$$

where AR represents the aspect ratio of the gold nanorods. Therefore, the predicted LSPR of nanorods

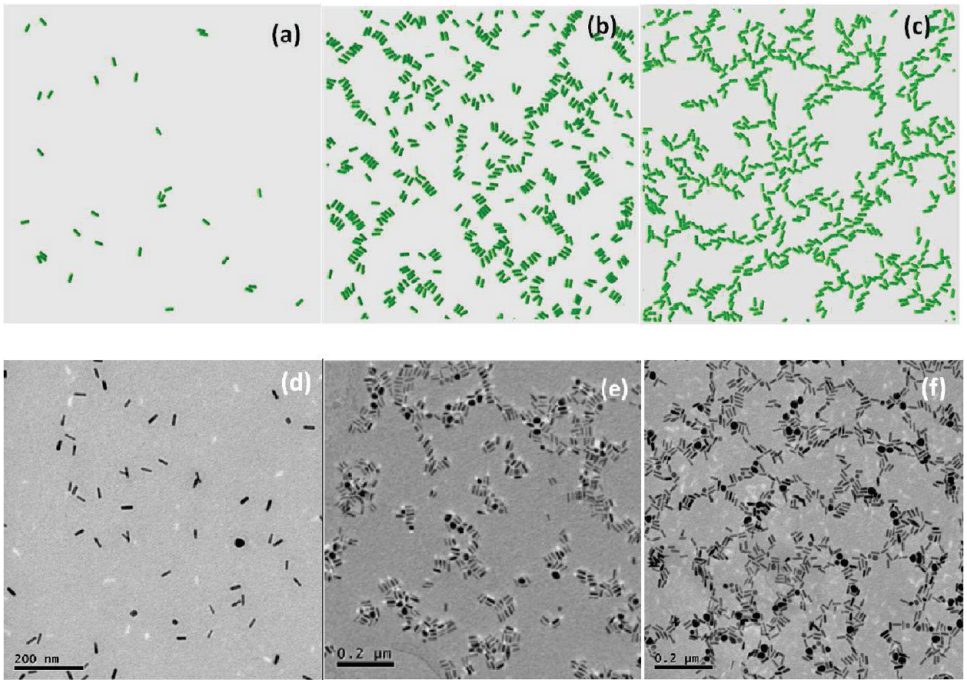

Figure 6. Monte Carlo simulations (a–c) and TEM images (d–f) of P2VP-AuNRs in P2VP films as a function of nanorod volume fraction. The MC values of $Ø_{AuNRs}$ are (a) 1.0%, (b) 15%, (c) 20% and experimental $Ø_{AuNRs}$ are (d) 0.4%, (e) 1.6%, and (f) 2.7%.

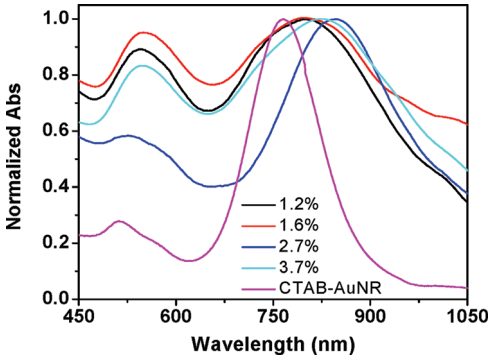

Figure 7. UV–vis spectra of CTAB-coated AuNRs in water and PVP-grafted AuNRs in P2VP films at $Ø_{AuNRs}$ of 1.2, 1.6, 2.7, and 3.7%. In the P2VP films, the LSPR red shifts from 801 to 846 nm as $Ø_{AuNRs}$ increases from 1.2 to 2.7% and then blue shifts upon further increasing $Ø_{AuNRs}$ to 3.7%. These shifts are attributed to the change in AuNR alignment described in Figure 3.

with AR ~ 3.6 is λ_{LSPR} = 764 nm, in very good agreement with experimental results.

Theoretical predictions and experimental studies show that the optical properties of AuNRs depend on the alignment and spacing of nanoparticles.[51–57] For example, polarization-dependent optical responses of spatially aligned nanorods in poly(vinyl alcohol) films has been demonstrated both experimentally and theoretically.[55] Figure 7 shows the UV–vis spectra of P2VP-AuNRs/P2VP films with compositions that are similar to the morphology in Figure 3. The positions of the TSPR and LSPR peaks are summarized in Table 1. At $Ø_{AuNRs}$ = 1.2%, the TSPR and LSPR are found at 544 and 801 nm, respectively. The corresponding morphology

TABLE 1. Summary of Transverse SPR, Longitudinal SPR Peak Positions in Water, and P2VP-AuNRs in P2VP Films

nanorod	TSPR (nm)	LSPR (nm)
AuNRs/H_2O	511	766
1.2%	544	801
1.6%	552	795
2.7%	526	846
3.7%	548	825

(Figure 3) contains 70% individual rods and 30% aggregates with mainly side-by-side nanorods. Upon increasing $Ø_{AuNRs}$ to 1.6%, the fraction of individual rods decreases, whereas the number of aggregates with side-by-side nanorods increases, leading to a red shift of the TSPR to 552 nm and a blue shift of the LSPR to 795 nm. By further increasing $Ø_{AuNRs}$ to 2.7%, a percolated network forms, with end-to-end nanorod linkages and fewer side-by-side nanorods. As a consequence, the TSPR undergoes a significant blue shift to 526 nm and the LSPR a red shift to 846 nm, respectively. At $Ø_{AuNRs}$ = 3.7%, the highest nanorod concentration, the TSPR peak returns to 548 nm and the LSPR shifts to 825 nm, indicating fewer end-to-end and more side-by-side aggregates compared to the morphology observed at the lower concentration, $Ø_{AuNRs}$ = 2.7%. The shifts in the TSPR and LSPR peak positions are in good agreement with simulations based on the discrete dipole approximation method.[50] El-Sayed *et al.*[51] proposed that the coupled nanorod plasmons can be considered as electromagnetic analogues of molecular orbitals. Thus, the end-to-end

nanorod plasmon coupling corresponds to a bonding state, while the side-by-side coupling corresponds to an antibonding state. Thus, by dispersing them in a polymer matrix, nanorod alignment can be controlled and, correspondingly, optical properties can be varied across the visible range of the spectrum.

SUMMARY AND CONCLUSIONS

In summary, we have explored the morphological evolution and optical properties of polymer nanocomposite films containing AuNRs grafted with brushes that are similar to the matrix. Control of the morphology is realized either by varying nanorod volume fraction at a fixed film thickness (~40 nm) or varying film thickness at a constant volume fraction (~2.7 vol %). In the former case, upon increasing $Ø_{AuNRs}$, the nanorod arrangements evolve from well-dispersed AuNRs to side-by-side aligned AuNRs in aggregates to end-to-end aligned AuNRs that bridge the aggregates. Polymer-induced depletion–attraction is responsible for the side-by-side alignment of nanorods. At $Ø_{AuNRs}$ = 2.7%, a continuous pathway is formed whereby the aggregates become linked by mainly end-to-end rods to form a percolated network. Upon fixing $Ø_{AuNRs}$ at 2.7%, the nanorod morphology evolves as polymer film thickness increases from 20 to 70 nm. Whereas nanorods in the thinnest polymer film, 20 nm, are well-dispersed, the nanorods in thicker films (40 and 70 nm) exhibit a percolated network.

Rutherford backscattering (RBS) measurements are conducted to evaluate the nanorod distribution as a function of depth. For thick films (~200 nm), nanorod concentration is enriched adjacent to the substrate. Monte Carlo simulations are performed to model the nanorod assembly as a function of nanorod loading. A qualitative comparison shows that the MC simulations are able to reproduce the structural evolution of the experimental morphologies observed by TEM as $Ø_{AuNRs}$ increases.

Finally, the correlation between nanorod structural morphology and optical properties has been illustrated. Nanorod side-by-side aggregation leads to a blue shift of the LSPR until $Ø_{AuNRs}$ reaches 1.6%. Upon increasing $Ø_{AuNRs}$ to 2.7%, a red shift of 51 nm is observed. Upon further increasing $Ø_{AuNRs}$, a blue shift of the LSPR is observed again. The optical properties of the nanocomposites vary in a systematic fashion, which renders these films attractive as smart coatings (*e.g.*, filters) or other sensing devices. In addition to their potential use as functional coatings, the percolated gold nanorods in a polymer matrix should lead to an enhancement in electrical conductivity and/or static charge dissipation while retaining its ability to form smooth films. In this sense, the combined advantages of controlling both optical and electrical properties should therefore open up new unique applications for these coatings. The present studies not only provide insight into how to control the assembly of anisotropic particles in a polymer matrix but also offer a better understanding of the structure–property relationship, which could guide intelligent design and fabrication of new optoelectronic devices.

METHODS

Materials and Sample Preparation. To study the assembly of AuNRs in polymer films, a poly(2-vinyl pyridine) thiol (P2VP-SH, M_n = 2500 g/mol) was used to functionalize AuNRs, which was then incorporated into a P2VP (M_n = 5000 g/mol) homopolymer film. The brush and matrix polymers were purchased from Polymer Source, Inc. (Montreal, Canada) and used as received without any purification. All reagents used in the synthesis of the nanorods were purchased from Sigma Aldrich and used as received. Milli-Q water (18.2 MΩ·cm^{-1}) was obtained from a Millipore water purification system. AuNRs were synthesized following the seeded growth method.[58,59]

Briefly, 1.7 mL of 0.1 M $HAuCl_4 \cdot 3H_2O$, 0.25 mL of $AgNO_3$, 0.27 mL of ascorbic acid, and 0.42 mL of a gold seed solution were added to 40 mL of 0.1 M hexadecyltrimethylammonium bromide (CTAB) and incubated at 40 °C for at least 3 h. The concentrations were chosen to maximize nanorod yield and resulted in nanorods with an average diameter of D_{rod} = 7.9 nm and length l_{rod} = 28.4 nm (aspect ratio ~3.6). After being centrifuged twice to remove excess CTAB from the solution at 10 000 rpm for 30 min each cycle, 0.3 mL of a highly concentrated AuNRs solution was added in 2 mL of a 2 mM ethanol solution of P2VP-SH and vigorously stirred at least 12 h. The reaction mixture was then transferred to methanol after centrifuging the concentrated solution at 10 000 rpm for 20 min and discarding the supernatant. After the second centrifugation, the P2VP-AuNRs were transferred to THF, which is another good solvent for P2VP. All polymer–nanorod thin films were prepared by spin-coating from the 0.5–3.0 wt % polymer/nanorod in THF solutions onto clean silicon or glass substrates. Spin rate was also varied from 1500 to 4000 rpm to tune film thicknesses. The silicon and glass substrates were precleaned with Piranha solution at 80 °C for 30 min. (*Caution: Piranha solution is prepared with 30 vol % H_2O_2/70 vol % H_2SO_4 and should be handled with extreme care under fume hood!*) The spin-cast films were then dried for 6 h in a vacuum oven. The resulting films had thicknesses ranging from 20 to 200 nm determined by ellipsometry, depending on the concentration of the polymer/nanorod solution.

Experimental Techniques. The UV–vis spectra of as-synthesized P2VP-AuNRs in different solvents (ethanol/H_2O, MeOH, and THF) and P2VP-AuNRs/P2VP homopolymer films were studied using Cary 5000 UV/vis spectrophotometer (Agilent). Assembly of AuNRs in P2VP homopolymer thin films was investigated by transmission electron microscopy (TEM) on a JEOL JEM 2010 at 200 kV. Specimens were prepared by floating the films from the silicon substrates onto a basic bath solution (pH ~10) and picking the films up on copper-coated carbon TEM grids (Electron Microscopy Sciences). TEM micrographs were processed in ImageJ to calculate the size of nanorods and the number of paired aggregates. Topography and phase images of P2VP-AuNRs/P2VP homopolymer films were measured by atomic force microscopy (Picoplus, Agilent Technologies) using tapping mode at frequencies around 190 Hz. AFM step height profile was used to determine the film thickness by scratching the film with a sharp razor blade. Rutherford backscattering spectrometry (RBS, NEC Corporation 5 SDH Pelletron) was used to extract the depth profile of gold in the nanocomposite films. For this study, a 2 MeV $4He^+$ ion beam was incident at 75° with

respect to the sample's normal surface. The total charge was 4 μC. XRUMP software (Genplot) was used to simulate RBS spectra and convert the energy scale to depth.

Monte Carlo Simulation of AuNRs Assembly. To model the morphology of our nanocomposites, we adopted a Monte Carlo (MC) model which simulates dispersions of polymer-functionalized nanoparticles in an implicit solvent using parameters obtained from classical density functional theory (DFT) calculations of nanorod−nanorod interaction strengths.[60] Under our implicit solvent approximation, nanoparticles interact *via* a potential:

$$U(h) = \begin{cases} \infty, h < h_{\min} \\ -\varepsilon, h_{\min} \le h \le h_c \\ 0, h > h_c \end{cases} \quad (3)$$

where h is the distance between the two nanorod surfaces, ε is the nanorod interaction energy, and the cutoff distance in terms of the nanorod radius is $h_c = r_{rod}$. The effect of the polymer brush on the AuNRs spacing is captured by h_{min}, which we take to be $0.28r_{rod}$. DFT calculations by Frischknecht[60] found that, for matrix molecular weights that are much larger than the brush molecular weight, $\varepsilon > 10k_BT$. Hence, we take this value as representative nanorod interaction energy in the MC simulations of our experimental systems. The nanorods are constructed from subparticles arranged in a face-centered cubic lattice with a lattice constant of $\alpha = 0.50r_{rod}$ and are randomly dispersed in a thin film with dimensions $256 \times 256 \times 2r_{rod}^3$. Following a short equilibration period, 4 MC moves are attempted with probabilities of 0.175:0.525:0.15:0.15. These moves correspond to rotation of nanorods, translation of nanorods, rotation of clusters of nanorods, and translation of clusters of nanorods, respectively. These moves are accepted according to the Metropolis algorithm at a temperature $T^* = k_BT$. To ensure the resulting morphology is not the product of statistical deviations, five independent runs are executed for each set of conditions. Our simulations were carried out in a massively parallel fashion using the compute unified device architecture (CUDA) libraries from NVIDIA.

Conflict of Interest: The authors declare no competing financial interest.

Acknowledgment. This work was supported by the National Science Foundation with primary support from the Polymer (DMR09-07493) and MRSEC (DMR11-20901) Programs. M.J.A.H. acknowledges support from NSF/IGERT (DGE-0221664). Secondary support was provided by NSF/NSEC (DMR08-32802).

Supporting Information Available: Determination of P2VP-AuNRs film thickness by the AFM scratching experiment and height profile; AFM height and phase images showing size and depth of the small depressions in the composite films when $\varnothing_{AuNRs}$ is 3.7%. This material is available free of charge *via* the Internet at http://pubs.acs.org.

REFERENCES AND NOTES

1. LeBaron, P. C.; Wang, Z.; Pinnavaia, T. J. Polymer-Layered Silicate Nanocomposites: An Overview. *Appl. Clay Sci.* **1999**, *15*, 11–29.
2. Gangopadhyay, R.; De, A. Conducting Polymer Nanocomposites: A Brief Overview. *Chem. Mater.* **2000**, *12*, 608–622.
3. Tseng, R. J.; Huang, J. X.; Ouyang, J.; Kaner, R. B.; Yang, Y. Polyaniline Nanofiber/Gold Nanoparticle Nonvolatile Memory. *Nano Lett.* **2005**, *5*, 1077–1080.
4. Jiang, G. Q.; Baba, A.; Ikarashi, H.; Xu, R. S.; Locklin, J.; Kashif, K. R.; Shinbo, K.; Kato, K.; Kaneko, F.; Advincula, R. Signal Enhancement and Tuning of Surface Plasmon Resonance in Au Nanoparticle/Polyelectrolyte Ultrathin Films. *J. Phys. Chem. C* **2007**, *111*, 18687–18694.
5. Harris, L. A.; Goff, J. D.; Carmichael, A. Y.; Riffle, J. S.; Harburn, J. J.; St Pierre, T. G.; Saunders, M. Magnetite Nanoparticle Dispersions Stabilized with Triblock Copolymers. *Chem. Mater.* **2003**, *15*, 1367–1377.
6. Moniruzzaman, M.; Winey, K. I. Polymer Nanocomposites Containing Carbon Nanotubes. *Macromolecules* **2006**, *39*, 5194–5205.
7. Wang, T. C.; Rubner, M. F.; Cohen, R. E. Polyelectrolyte Multilayer Nanoreactors for Preparing Silver Nanoparticle Composites: Controlling Metal Concentration and Nanoparticle Size. *Langmuir* **2002**, *18*, 3370–3375.
8. Ramesh, G. V.; Porel, S.; Radhakrishnan, T. P. Polymer Thin Films Embedded with *In Situ* Grown Metal Nanoparticles. *Chem. Soc. Rev.* **2009**, *38*, 2646–2656.
9. Patton, D.; Locklin, J.; Meredith, M.; Xin, Y.; Advincula, R. Nanocomposite Hydrogen-Bonded Multilayer Ultrathin Films by Simultaneous Sexithiophene and Au Nanoparticle Formation. *Chem. Mater.* **2004**, *16*, 5063–5070.
10. Shenhar, R.; Norsten, T. B.; Rotello, V. M. Polymer-Mediated Nanoparticle Assembly: Structural Control and Applications. *Adv. Mater.* **2005**, *17*, 657–659.
11. Gupta, S.; Zhang, Q. L.; Emrick, T.; Russell, T. P. "Self-Corralling" Nanorods under an Applied Electric Field. *Nano Lett.* **2006**, *6*, 2066–2069.
12. Mitamura, K.; Imae, T.; Saito, N.; Takai, O. Fabrication and Self-Assembly of Hydrophobic Gold Nanorods. *J. Phys. Chem. B* **2007**, *111*, 8891–8898.
13. Sun, B. Q.; Sirringhaus, H. Surface Tension and Fluid Flow Driven Self-Assembly of Ordered ZnO Nanorod Films for High-Performance Field Effect Transistors. *J. Am. Chem. Soc.* **2006**, *128*, 16231–16237.
14. Ahmed, S.; Ryan, K. M. Self-Assembly of Vertically Aligned Nanorod Supercrystals Using Highly Oriented Pyrolytic Graphite. *Nano Lett.* **2007**, *7*, 2480–2485.
15. Baker, J. L.; Widmer-Cooper, A.; Toney, M. F.; Geissler, P. L.; Alivisatos, A. P. Device-Scale Perpendicular Alignment of Colloidal Nanorods. *Nano Lett.* **2010**, *10*, 195–201.
16. Guerrero-Martínez, A.; Pérez-Juste, J.; Carbó-Argibay, E.; Tardajos, G.; Liz-Marzán, L. M. Gemini-Surfactant-Directed Self-Assembly of Monodisperse Gold Nanorods into Standing Superlattices. *Angew. Chem., Int. Ed.* **2010**, *121*, 9648–9652.
17. Wang, H. F.; Huff, T. B.; Zweifel, D. A.; He, W.; Low, P. S.; Wei, A.; Cheng, J. X. *In Vitro* and *In Vivo* Two-Photon Luminescence Imaging of Single Gold Nanorods. *Proc. Natl. Acad. Sci. U.S.A.* **2005**, *102*, 15752–15756.
18. Huff, T. B.; Tong, L.; Zhao, Y.; Hansen, M. N.; Cheng, J. X; Wei, A. Hyperthermic Effects of Gold Nanorods on Tumor Cells. *Nanomedicine* **2007**, *2*, 125–132.
19. Chen, C. D.; Cheng, S. F.; Chau, L. K.; Wang, C. R. C. Sensing Capability of the Localized Surface Plasmon Resonance of Gold Nanorods. *Biosens. Bioelectron.* **2007**, *22*, 926–932.
20. Orendorff, C. J.; Gearheart, L.; Jana, N. R.; Murphy, C. J. Aspect Ratio Dependence on Surface Enhanced Raman Scattering Using Silver and Gold Nanorod Substrates. *Phys. Chem. Chem. Phys.* **2006**, *8*, 165–170.
21. Zhang, Q. L.; Gupta, S.; Emrick, T.; Russell, T. P. Surface-Functionalized CdSe Nanorods for Assembly in Diblock Copolymer Templates. *J. Am. Chem. Soc.* **2006**, *128*, 3898–3899.
22. Deshmukh, R. D.; Liu, Y.; Composto, R. J. Two-Dimensional Confinement of Nanorods in Block Copolymer Domains. *Nano Lett.* **2007**, *7*, 3662–3668.
23. Son, J. G.; Bae, W. K.; Kang, H. M.; Nealey, P. F.; Char, K. Placement Control of Nanomaterial Arrays on the Surface-Reconstructed Block Copolymer Thin Films. *ACS Nano* **2009**, *3*, 3927–3934.
24. Xu, C.; Ohno, K.; Ladmiral, V.; Milkie, D. E.; Kikkawa, J. M.; Composto, R. J. Simultaneous Block Copolymer and Magnetic Nanoparticle Assembly in Nanocomposite Films. *Macromolecules* **2009**, *42*, 1219–1228.
25. Deshmukh, R. D.; Buxton, G. A.; Clarke, N.; Compsoto, R. J. Nanoscale Block Copolymer Templates Decorated by Nanoparticle Arrays. *Macromolecules* **2007**, *40*, 6316–6324.
26. Hore, M. J. A.; Composto, R. J. Nanorod Self-Assembly for Tuning Optical Absorption. *ACS Nano* **2010**, *4*, 6941–6949.
27. Sciancalepore, C.; Cassano, T.; Curri, M. L.; Mecerreyes, D.; Valentini, A.; Agostiano, A.; Tommasi, R.; Striccoli, M. TiO_2 Nanorods/PMMA Copolymer-Based Nanocomposites: Highly Homogeneous Linear and Nonlinear Optical Material. *Nanotechnology* **2008**, *19*, 205705.

28. Zhang, Q. L.; Russell, T. P.; Emrick, T. Synthesis and Characterization of CdSe Nanorods Functionalized with Regioregular Poly(3-hexylthiophene). *Chem. Mater.* **2007**, *19*, 3712–3716.
29. Du, F. M.; Fischer, J. E.; Winey, K. I. Effect of Nanotube Alignment on Percolation Conductivity in Carbon Nanotube/Polymer Composites. *Phys. Rev. B* **2005**, *72*, 121404.
30. Du, F.; Scogna, R. C.; Zhou, W.; Brand, S.; Fischer, J. E.; Winey, K. I. Nanotube Networks in Polymer Nanocomposites: Rheology and Electrical Conductivity. *Macromolecules* **2004**, *37*, 9048–9055.
31. Park, K.; Koerner, H.; Vaia, R. A. Depletion-Induced Shape and Size Selection of Gold Nanoparticles. *Nano Lett.* **2010**, *10*, 1433–1439.
32. Sharma, V.; Oosawa, F. On Interaction between Two Bodies Immersed in a Solution of Macromolecules. *J. Chem. Phys.* **1954**, *22*, 1255–1256.
33. Vigolo, B.; Coulon, C.; Maugey, M.; Zakri, C.; Poulin, P. An Experimental Approach to the Percolation of Sticky Nanotubes. *Science* **2005**, *309*, 920–923.
34. Jungblut, S.; Tuinier, R.; Binder, K.; Schilling, T. Depletion Induced Isotropic−Isotropic Phase Separation in Suspensions of Rod-like Colloids. *J. Chem. Phys.* **2007**, *127*, 244909(1−9).
35. Surve, M.; Pryamitsyn, V.; Ganesan, V. Dispersion and Percolation Transitions of Nanorods in Polymer Solutions. *Macromolecules* **2007**, *40*, 344–354.
36. Kyrylyuk, A. V.; van der Schoot, P. Continuum Percolation of Carbon Nanotubes in Polymeric and Colloidal Media. *Proc. Natl. Acad. Sci. U.S.A.* **2008**, *105*, 8221–8226.
37. Huynh, W. U.; Dittmer, J. J.; Alivisatos, A. P. Hybrid Nanorod-Polymer Solar Cells. *Science* **2002**, *295*, 2425–2427.
38. Liu, Y.; Mills, E. N.; Composto, R. J. Tuning Optical Properties of Gold Nanorods in Polymer Films through Thermal Reshaping. *J. Mater. Chem.* **2009**, *19*, 2704–2709.
39. Surve, M.; Pryamitsyn, V.; Ganesan, V. Nanoparticles in Solutions of Adsorbing Polymers: Pair Interactions, Percolation, and Phase Behavior. *Langmuir* **2006**, *22*, 969–981.
40. Ganesan, V.; Ellison, C. J.; Pryamitsyn, V. Mean-Field Models of Structure and Dispersion of Polymer−Nanoparticle Mixtures. *Soft Matter* **2010**, *6*, 4010–4025.
41. Surve, M.; Pryamitsyn, V.; Ganesan, V. Dispersion and Percolation Transitions of Nanorods in Polymer Solutions. *Macromolecules* **2007**, *40*, 344–354.
42. Hore, M. J. A.; Composto, R. J. Nanorod Assemblies in Polymer Films and Their Dispersion-Dependent Optical Properties. *ACS Macro Lett.* **2012**, *1*, 115–121.
43. Kim, K. D.; Sperling, L. H.; Klein, A.; Wignall, G. D. Characterization of Film Formation from Direct Miniemulsified Polystyrene Latex Particles *via* SANS. *Macromolecules* **1993**, *26*, 4624–4631.
44. Schilling, T.; Jungblut, S.; Miller, M. A. Depletion-Induced Percolation in Networks of Nanorods. *Phys. Rev. Lett.* **2007**, *98*, 108303(1−4).
45. Kim, S. H.; Misner, M. J.; Xu, T.; Kimura, M.; Russell, T. P. Highly Oriented and Ordered Arrays from Block Copolymers *via* Solvent Evaporation. *Adv. Mater.* **2004**, *16*, 226–231.
46. Sun, S. H.; Anders, S.; Hamann, H. F.; Thiele, J. U.; Baglin, J. E. E.; Thomson, T.; Fullerton, E. E.; Murray, C. B.; Terris, B. D. Polymer Mediated Self-Assembly of Magnetic Nanoparticles. *J. Am. Chem. Soc.* **2002**, *124*, 2884–2885.
47. Faupel, F.; Willecke, R.; Thran, A. Diffusion of Metals in Polymers. *Mater. Sci. Eng., R* **1998**, *22*, 1–55.
48. Composto, R. J.; Walters, R. M.; Genzer, J. Application of Ion Scattering Techniques To Characterize Polymer Surfaces and Interfaces. *Mater. Sci. Eng., R* **2002**, *38*, 107–180.
49. Gam, S.; Meth, J. S.; Zane, S. G.; Chi, C. Z.; Wood, B. A.; Seitz, M. E.; Winey, K. I.; Clarke, N.; Composto, R. J. Macromolecular Diffusion in a Crowded Polymer Nanocomposite. *Macromolecules* **2011**, *44*, 3494–3501.
50. Brioude, A.; Jiang, X. C.; Pileni, M. P. Optical Properties of Gold Nanorods: DDA Simulations Supported by Experiments. *J. Phys. Chem. B* **2005**, *109*, 13138–13142.
51. Jain, P. K.; Eustis, S.; El-Sayed, M. A. Plasmon Coupling in Nanorod Assemblies: Optical Absorption, Discrete Dipole Approximation Simulation, and Exciton-Coupling Model. *J. Phys. Chem. B* **2006**, *110*, 18243–18253.
52. Funston, A. M.; Novo, C.; Davis, T. J.; Mulvaney, P. Plasmon Coupling of Gold Nanorods at Short Distances and in Different Geometries. *Nano Lett.* **2009**, *9*, 1651–1658.
53. Chang, J. Y.; Wu, H. M.; Chen, H.; Ling, Y. C.; Tan, W. H. Oriented Assembly of Au Nanorods Using Biorecognition System. *Chem. Commun.* **2005**, *8*, 1092–1094.
54. Wang, L. B.; Zhu, Y. Y.; Xu, L. G.; Chen, W.; Kuang, H.; Liu, L. Q.; Agarwal, A.; Xu, C. L.; Kotov, N. A. Side-by-Side and End-to-End Gold Nanorod Assemblies for Environmental Toxin Sensing. *Angew. Chem., Int. Ed.* **2010**, *49*, 5472–5475.
55. Perez-Juste, J.; Rodriguez-Gonzalez, B.; Mulvaney, P.; Liz-Marzan, L. M. Optical Control and Patterning of Gold-Nanorod-Poly(vinyl alcohol) Nanocomposite Films. *Adv. Funct. Mater.* **2005**, *15*, 1065–1071.
56. Murphy, C. L.; Orendorff, C. J. Alignment of Gold Nanorods in Polymer Composites and on Polymer Surfaces. *Adv. Mater.* **2005**, *17*, 2173–2177.
57. Li, J.; Liu, S.; Liu, Y.; Zhou, F.; Li, Z. Y. Anisotropic and Enhanced Absorptive Nonlinearities in a Macroscopic Film Induced by Aligned Gold Nanorods. *Appl. Phys. Lett.* **2010**, *96*, 263103.
58. Sau, T. K.; Murphy, C. J. Seeded High Yield Synthesis of Short Au Nanorods in Aqueous Solution. *Langmuir* **2004**, *20*, 6414–6420.
59. Nikoobakht, B.; El-Sayed, M. A. Preparation and Growth Mechanism of Gold Nanorods (AuNRs) Using Seed-Mediated Growth Method. *Chem. Mater.* **2003**, *15*, 1957–1962.
60. Frischknecht, A. L. Forces between Nanorods with End-Adsorbed Chains in a Homopolymer Melt. *J. Chem. Phys.* **2008**, *128*, 224902.